POLITECNICO DI TORINO
Repository ISTITUZIONALE

An Analytical Model for Performance Estimation in Modern High-Capacity IMDD Systems

Original
An Analytical Model for Performance Estimation in Modern High-Capacity IMDD Systems / Rizzelli, G., Torres-Ferrera, P., Forghieri, F., Gaudino, R.. - In: JOURNAL OF LIGHTWAVE TECHNOLOGY. - ISSN 0733-8724. - STAMPA. - 42:5(2024), pp. 1443-1452. [10.1109/jlt.2023.3324260]

Availability:
This version is available at: 11583/2991973 since: 2024-11-07T09:45:15Z

Publisher:
IEEE

Published
DOI:10.1109/jlt.2023.3324260

Terms of use:

This article is made available under terms and conditions as specified in the corresponding bibliographic description in the repository

Publisher copyright
IEEE postprint/Author's Accepted Manuscript

©2024 IEEE. Personal use of this material is permitted. Permission from IEEE must be obtained for all other uses, in any current or future media, including reprinting/republishing this material for advertising or promotional purposes, creating new collecting works, for resale or lists, or reuse of any copyrighted component of this work in other works.

(Article begins on next page)

14 October 2026

An Analytical Model for Performance Estimation in Modern High-Capacity IMDD Systems

Giuseppe Rizzelli, Pablo Torres-Ferrera, Fabrizio Forghieri, *Fellow, IEEE* and Roberto Gaudino, *Senior Member, IEEE*

***Abstract*—In this Paper, we propose an analytical model to estimate the signal-to-noise ratio (SNR) and then the Bit Error Rate (BER) at the output of a receiver adaptive equalizer in intensity modulation and direct detection (IMDD) optical transmission systems affected by optoelectronic bandwidth limitations, chromatic dispersion (CD), quantization noise, relative intensity noise (RIN), shot noise and thermal noise. We consider that the proposed model is a powerful tool for the numerical design of strongly band-limited IMDD systems using receiver equalization, as it happens in most of modern and future M-PAM solutions for short reach and access systems. We develop the model as an extension of a previously presented one, and then we test its accuracy by sweeping the main parameters of a 4-PAM-based communication system, such as RIN coefficient, extinction ratio (ER), accumulated CD, equalizer type and memory. Our findings show a remarkable agreement between time-domain simulations and analytical results, with SNR discrepancies below 0.1 dB in most cases, for both feed-forward and decision-feedback equalization. Moreover, we tested our model predictions against experimental measurements, confirming its accuracy.**

***Index Terms*—Intensity Modulation, Direct Detection, Optical Communications, Performance Modeling.**

I. Introduction

THE market volume for short-reach and access network transceivers is continuously growing and, in parallel, the data rate requests are more and more demanding. Although coherent detection (CoD) is making its way at the research level into shorter transmission reach segments [1]–[6], IMDD systems are still the solution of choice in most of the metro edge and access networks applications, as well as in many intra- and inter- data center interconnects (DCI) [6]–[11]. Modern IMDD-based standards are today increasingly relying on more advanced modulation formats than the traditional binary on-off keying (OOK) in order to improve legacy systems performance and thus extend their lifespan in an increasingly data-hungry society. For instance, the 400GBASE-LR4 and the 400GBASE-SR standards have defined solutions for SMF-based short-reach and VCSEL+MMF-based DCI links, respectively, relying on 4-PAM modulation to reach up to 100 Gbps/λ.

As it is the case for the design or analysis of any transmission system, the possibility to numerically predict the performance of an IMDD system can be of great help in the effort to efficiently plan and optimize network capacity at the physical layer. This is usually achieved through computationally intensive simulations in the time domain that allow to estimate, for instance, the bit error ratio (BER) of the end-to-end physical layer system for a given set of fixed parameters. However, such a CPU time consuming approach can be highly impractical when the optimization of a great number of parameters is required as, for instance, in a multi-dimensional Monte Carlo analysis [12] or in a statistical analysis [11].

In a recent paper [13], we presented an analytical tool for performance prediction applied to a coherent system considering dual polarization transmission, a linear channel described by a [2x2] frequency dependent transfer function, colored additive Gaussian noise at the receiver and a full digital signal processing (DSP) implementation at the receiver. The proposed model [13] allows for over 300 times reduction in computation time with respect to a full time domain simulation generating a single BER or SNR estimate in less than 0.05 seconds on a standard commercial laptop. In this new contribution, we propose a similar approach but specifically tailored to modern IMDD systems using receiver equalization and without optical amplification. In particular, the new model presented in this Paper allows to compute the electrical SNR at the equalizer output in an IMDD scheme with M-PAM modulation, considering different sources of impairments such as optoelectronic bandwidth limitations, RIN associated to the transmitter laser, fiber chromatic dispersion, shot noise due to photodection, thermal noise of the transimpedence amplifiers (TIA) and quantization noise of the analog-to-digital converters (ADC) at the receiver, and equalizer implementation. Once the electrical SNR is evaluated, we also show how to estimate the resulting BER for a given M-PAM format. Compared to existing time-domain performance estimation tools, our approach enables fast and accurate performance prediction of modern IMDD systems affected by a broad variety of impairments.

As for our previously published coherent analytical model [13], also the IMDD model proposed here is based on the work by Robert Fischer [14] and it is suitable only for linear channels. In both cases, we had to significantly modify the original Fischer's model to the different requirement of the two classes of optical systems. In particular, for the coherent case, propagation can be described through an additive white Gaussian noise (AWGN) channel on the optical field complex envelope signal, and similarly optoelectronic bandwidth

G. Rizzelli is with the LINKS Foundation, Torino, Italy, e-mail: giuseppe.rizzelli@linksfoundation.com.

P. Torres-Ferrera is with the Department of Engineering, University of Cambridge, Cambridge, United Kingdom. Prior, he was with the Department of Electronics and Telecommunications, Politecnico di Torino, Torino, Italy.

F. Forghieri is with CISCO Photonics Italy, Vimercate, Italy.

R. Gaudino is with the Department of Electronics and Telecommunications, Politecnico di Torino, Torino, Italy.

limitations are suitably modeled as transfer functions on the optical field. The situation for (not optically amplified) IMDD system is indeed quite different since:

- signal evolution is better treated in terms of instantaneous power $P(t)$ in the fiber, and then as electrical signals $i_{RX}(t)$ that are proportional to $P(t)$ (through receiver responsivity and gain);
- optoelectronic bandwidth limitation can be modeled as linear transfer function on either $P(t)$ or $i_{RX}(t)$. The notable exception is the impact of chromatic dispersion (which is linear on the field representation of the signal, and not on $P(t)$)
- all noise sources are typically additive on either $P(t)$ or $i_{RX}(t)$;
- while the transimpedance amplifier noise typically has a constant variance, other important noise sources are actually signal dependent. Specifically, the RIN variance is proportional to $P^2(t)$, while the shot noise one scales with $P(t)$

The specific novelty of our approach is indeed in heuristically adapting the tool presented in [14] to include all these specific IMDD characteristics for signal propagation and noise addition. To describe our proposal, we start in this paper by introducing the key equations and assumptions behind our new model and then we validate it by comparing its performance prediction against fully-fledged (and very CPU-intensive) time-domain simulations based on error counting and show the estimation error in terms of both SNR and BER at the equalizer output. The validation is performed on a set of physical layer parameters that are typical of modern DCI-interconnect systems or access networks.

An open-access free version of the Matlab code implementing the presented analytical model can be found in [15], [16].

The remainder of this manuscript is organized as follows: in Section II we describe the analytical model, defining the assumptions and showing the main equations. In Section III we then report on the comparison between the analytical model performance estimation and a comprehensive set of time domain simulations, highlighting its accuracy in a 4-PAM-based transmission system under several typical short-reach PAM-M modern applications. In Section IV we focus on specific application scenarios and apply our model to a passive optical networks (PON) in O-band, including CD and APD-based detection, and compare it to both simulation and experimental results. Moreover we test the model in a DCI transmission based on MMF and VCSEL. Lastly, in Section V we summarize the main results and draw some conclusion.

II. The proposed analytical model

A simplified block diagram of the system under investigation is depicted in Fig. 1, where the signals in the different sections are either given in terms of instantaneous power in the fiber or in the (linearly proportional) electrical signals after the photodetecion process. We start in the schematic of Fig. 1 from the transmitter that generates the M-PAM modulated signal and also includes a shaping filtering stage indicated by the transfer function $H_T(f)$. For simplicity, we will show numerical examples assuming a rectangular shape for the transmitted symbols in the time domain, but any other shape can also be handled analytically. Moreover, although our approach can be applied to any M-PAM format, we will focus most of our following application examples on 4-PAM modulation. We assume that the RIN at the transmitter can be modeled as a noise source with variance $\sigma^2_{RIN} = k_{RIN} \cdot P^2_{TX}(t)$ proportional to the average transmitted power squared, added at the transmitter before the signal is filtered by a linear channel with end-to-end transfer function $H_{ch}(f)$. The channel can be described by a generic frequency response of any type, but in this work we use a supergaussian profile of variable order. Please note that $H_{ch}(f)$ thus acts also on the power spectral density (PSD) of the RIN. At the receiver side the (electrical) signal receives the contributions of thermal and shot noise with PSDs $S_{th} = N_0/2$ and $S_{shot} = k_{shot} \cdot P_{RX}(t)$, respectively. The receiver, after an ADC, is equipped with two possible Minimum Mean-Square Error (MMSE)-based equalization schemes, a feedforward equalizer (FFE) and a decision feedback equalizer (DFE). In the time domain simulator, the BER is then computed through an error counting technique and the SNR calculated as the ratio of the average energy of the signal to the mean square error at the output of the equalizer (at one sample per PAM-M symbol).

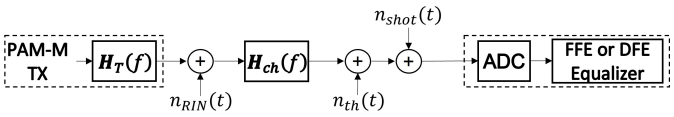

Fig. 1. Block diagram of the system under investigation with noise sources.

In [14], the Author proposed an analytical model (that we will indicate in the following as the Fischer's model) for the estimation of the SNR at the equalizer output, given a generic linear transfer function $H_{ch}(f)$, under two main assumptions: i) the channel is a bandlimited AWGN with generic transfer function and ii) the equalizer is infinitely long. A more detailed description of the model can be found in [14] or [13]. Here, we just recall the key equations of the original Fischer's model, which is based on the spectrally resolved $SNR(f)$ at the equalizer input, computed as:

$$SNR(f) = \frac{T \cdot P_{TX} \cdot |H_T(f) \cdot H_{ch}(f)|^2}{N_0(f)} \tag{1}$$

where T is the symbol period, P_{TX} is the transmitted signal power expressed in W, $H_{ch}(f)$ is the linear channel transfer function, $H_T(f)$ is the transfer function of the transmitter shaping filter and $N_0(f)$ is the equivalent noise power spectral density at the input of the receiver expressed in W/Hz. The SNR at the output of the infinitely long equalizer is then computed as:

$$SNR_{FFE} = \frac{1}{T \cdot \int_{-\frac{1}{2T}}^{\frac{1}{2T}} \frac{1}{\overline{SNR}(f)+1} df} - 1 \tag{2}$$

$$SNR_{DFE} = e^{T \cdot \int_{-\frac{1}{2T}}^{\frac{1}{2T}} log[\overline{SNR}(f)+1] df} - 1 \tag{3}$$

respectively for FFE and DFE equalization, where $\overline{SNR}(f)$ is the spectral $SNR(f)$ folded on a bandwidth equal to the symbol rate (due to the analog-to-digital conversion process in front of the equalizer), defined as:

$$\overline{SNR}(f) = \sum_{\mu} SNR(f - \frac{\mu}{T}) \tag{4}$$

where the integer μ indicates the number of foldings.

In the IMDD scenario that we want to address here we can still use Equations 2-4, but we need to carefully modify Eq. 1, as explained below. A first key characteristic of IMDD signal propagation according to the schematic reported in Fig. 1 is the representation of the modulated signal in terms of instantaneous power. For an M-PAM modulated signal we can write the instantaneous transmitted power as:

$$P_{TX}(t) = \overline{P_{TX}} + \frac{OMA_{TX}^{outer}}{2 \cdot (M-1)} \cdot \sum_{k=-\infty}^{+\infty} \alpha_k \cdot s(t - kT) \tag{5}$$

where OMA_{TX}^{outer} is the outer Optical Modulation Amplitude (OMA) in W, α_k is a random variable taking one of the M-PAM levels (e.g. $[-3, -1, 1, 3]$ for 4-PAM) and $s(t - kT)$ is the pulse shape. The resulting power spectral density (PSD) of the (useful part of the) transmitted signal expressed in W^2/Hz is thus (neglecting the irrelevant DC component in $f = 0$):

where $\sigma^2_{\alpha_k} = \Sigma\alpha_k^2/M$ and $|H_T(f)|^2$ is the spectral shape of the transmitted signal. The ER, defined as the ratio between the high and low power levels, is related to the outer OMA through the equation:

$$OMA^{outer} = 2 \cdot \overline{P_{TX}} \cdot \frac{(ER-1)}{(ER+1)} \tag{6}$$

Let us now focus on the evaluation of the noise PSD at the equalizer input (expressed in W^2/Hz), which we write as the sum of the (statistically independent) contribution of four noise sources (RIN, shot, thermal and quantization noise) as:

$$S_N(f) = S_{RIN} \cdot |H_{ch}(f)|^2 + S_{shot}(f) + S_{th}(f) + S_{ADC}(f) \tag{7}$$

where:

- $S_{th}(f)$ is the PSD of the additive thermal noise, typically due to the internal noise generated by the TIA and usually signal-power independent (but possibly frequency-dependent, i.e. colored additive Gaussian noise)
- S_{RIN} is the PSD of the RIN noise, which we evaluate as $S_{RIN} = k_{RIN} \cdot \overline{P_{TX}^2}$, where $\overline{P_{TX}^2}$ is the average transmitted optical power squared and $k_{RIN} = RIN_{coeff}/2$ is a proportionality factor that depends on the RIN coefficient RIN_{coeff} expressed in $1/Hz$
- $S_{shot}(f)$ is the PSD of the shot noise, which we evaluate as $S_{shot} = k_{shot} \cdot \overline{P_{RX}}$ where $\overline{P_{RX}}$ is the average received optical power and $k_{shot} = G^2 F q R^{-1}$ is a proportionality factor that depends on the photodetector excess noise figure F, the photodetector gain G (when considering avalanche photodetection, whereas for a PIN photodiode $G = F = 1$), the photodiode responsivity R and the electron charge q.
- $S_{ADC}(f)$ is the PSD of the quantization noise expressed as [22]:

$$S_{ADC}(f) = \frac{PAPR \cdot \sigma_x^2}{12 \cdot f_s \cdot 2^{(2 \cdot ENOB - 2)}} \tag{8}$$

where PAPR is the peak to average power ratio, ENOB and f_s are the effective number of bits and sampling frequency of the oscilloscope, respectively, and $\sigma_x^2 = \int_{-f_s/2}^{f_s/2} S_x(f) df$ is the power of the AC-coupled signal after quantization.

The introduction of $\overline{P_{TX}^2}$ and $\overline{P_{RX}}$ in the evaluation of RIN and shot noise, respectively, is the first approximation of our model, since our tool is frequency resolved and we cannot analytically account for the instantaneous time dependence of the noise level.

In conclusion, focusing on the equations for a 4-PAM modulated signal, using the modifications to Eq. 1 represented by Eqs. 5, **??** and 7, and the approximations on the RIN and shot noise PSD, we obtain the following expression for the spectral SNR:

$$SNR(f) = \frac{5}{36} \cdot \frac{T \cdot (OMA_{TX}^{outer})^2 \cdot |H_T(f)|^2 \cdot |H_{ch}(f)|^2}{S_N(f)} \tag{9}$$

For the three main noise contributions in the time domain simulator we define the time-dependent variances $\sigma_{th}^2 = N_0 \cdot f_s/2$, $\sigma_{shot}^2(t) = 2G^2 F q R^{-1} P_{RX}(t) \cdot f_s/2$ and $\sigma_{RIN}^2(t) = RIN_{coeff} P_{TX}^2(t) \cdot f_s/2$, where f_s is the simulator sampling frequency. As we want to focus first on the impact of the fundamental noise contributions, the effect of the quantization noise is included only in the comparison with experimental measurements in Section IV-B.

As a first example of application of the proposed model, Fig. 2a shows a comparison of the results obtained with the time domain simulator and with the proposed analytical model in terms of SNR at the equalizer output as a function of the ratio between the $H_{ch}(f)$ supergaussian filter 3 dB bandwidth (B_{3dB}) and the symbol rate (R_s) for a 25 GBaud 4-PAM system, using both FFE and DFE equalization. The order of the supergaussian filter is set to 1 or 3. The complete set of simulation parameters are shown in Table I. These are the parameters used throughout the paper unless otherwise specified. For this preliminary comparison between the simulator and the model based on the infinitely long equalizer assumption, in this first model performance validation, we set a high number of taps in the simulator equalizers, respectively 200 for the FFE and 30 for the DFE stage operated in full-training mode (we will come back on this somehow idealized assumption in one of the following Sections, showing that the accuracy is good also for a much smaller number of equalizer taps). Fig. 2a shows a very good agreement between the two methods with maximum estimation error of the order of 0.05 dB, regardless of the filter order and of the introduced bandwidth limitations, for both equalization schemes.

Once an SNR value is numerically obtained, it is then possible to estimate the resulting BER using the following BER formula, which is valid for a generic M-PAM modulation in additive Gaussian noise:

$$BER \simeq \frac{M-1}{M \cdot log_2(M)} \mathrm{erfc}\left(\sqrt{\frac{3 \cdot SNR}{2(M^2-1)}}\right) \tag{10}$$

TABLE I
SIMULATION PARAMETERS.

Parameter	Value	Unit
Symbol Rate	25	GBaud
RIN	-140	dB/Hz
Extinction Ratio	6	dB
OMA	0.78	dBm
Responsivity	1	A/W
P_{TX}	1	mW
N_0	$2 \cdot 10^{-19}$	W^2/Hz
FFE (DFE) Taps	200 (30)	

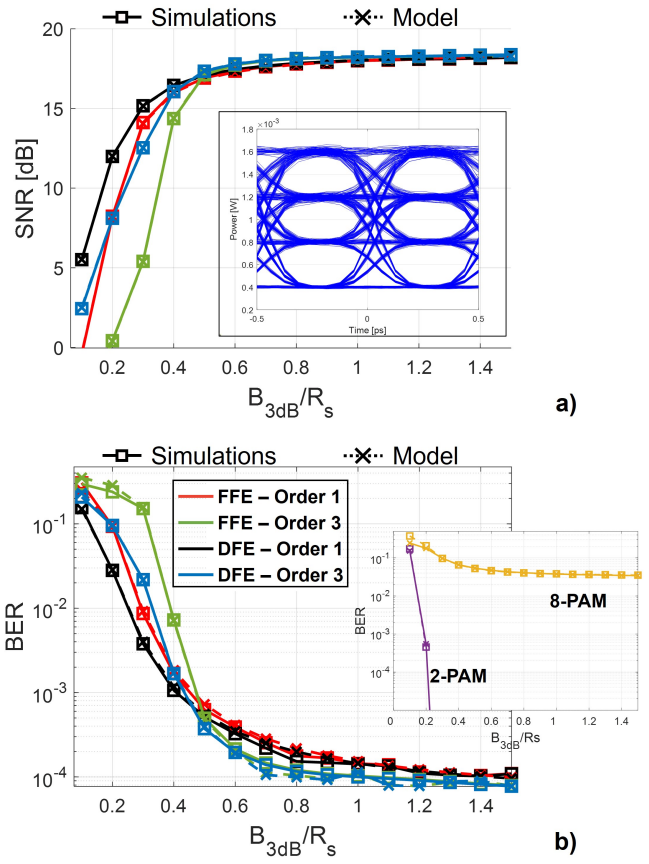

Fig. 2. a) SNR and b) BER obtained through time domain simulations (solid, squares) and through the proposed analytical model (dashed, crosses) as a function of the ratio between the supergaussian filter 3 dB bandwidth B_{3dB} and the symbol rate R_s for a 25 GBaud 4-PAM system, using both FFE (red and green) and DFE (black and blue) equalization. The supergaussian filter order is 1 for black and red curves and 3 for blue and green curves. The inset in a) shows the eye diagram of the 4-PAM signal after the channel filtering when $B_{3dB}/R_s = 0.8$. The inset in b) shows results also for FFE-based 2-PAM (purple) and 8-PAM (orange) modulation with supergaussian filter order 1. The legend in b) applies to a) as well.

where M is the constellation size. When noise sources are signal-dependent (as for RIN and shot noise), this formula cannot be directly used since, as shown in the inset of Fig. 2a, the resulting 4-PAM eye diagram highlights a stronger effect of the RIN (and shot noise) on the upper eyes corresponding to a higher instantaneous power. We thus proposed, and then verified *a posteriori* the following heuristic upgrade to the previously presented model for the evaluation of the BER:

- we evaluate the SNR on each of the three inner eye-diagrams for 4-PAM, using a RIN and shot noise variance corresponding to the average power related to each of the inner eye-diagrams;
- we evaluate the corresponding three BER values using Eq. 10;
- we approximate the global BER as the average among these three BER values. Consequently, when the system is limited by RIN rather than TIA thermal noise, the overall BER is actually dominated by the lowest among the three SNRs of each of the three inner eye-diagrams. In the following Section IIIA we will perform a detailed analysis of the proposed heuristic SNR-to-BER conversion also in extreme RIN conditions.

We show in Fig. 2b the BER obtained in the same conditions as in Fig. 2a, compared to the BER computed in the simulations through error counting. Fig. 2b shows an excellent agreement of the analytical model with the time domain simulations, also in terms of BER, at least in the BER range of interest down to 10^{-4} (to obtain this figure the BER counting simulator operates on about $5 \cdot 10^5$ bits and, therefore, it becomes inaccurate for BER below 10^{-5}). The inset in Fig. 2b shows a very good BER agreement also for FFE-based 25 GBaud 2-PAM and 8-PAM modulations with super-Gaussian filter order 1, confirming that the model can be applied to any M-PAM format. Similar results are obtained for DFE equalization as well (not shown due to space limitations). In terms of CPU time, a pair of SNR values for the two equalization schemes can be obtain in about 0.045 seconds through the analytical model on a commercial standard laptop PC which, compared to the 18.5 seconds needed to run the time domain simulation, thus the model yields a ~400 times reduction in computational time.

III. FURTHER VALIDATIONS AND EXTENSION OF THE PROPOSED MODEL UNDER DIFFERENT OPERATING CONDITIONS

In this Section, we check the validity of the model in different scenarios, extending the analysis to higher bit rates and to somewhat "extreme" RIN conditions. Then, we extend its applicability including the effect of chromatic dispersion and APD-induced shot noise, and of finite memory in equalizer internal FIR filters. Hereafter, the bandlimited channel is described by a supergaussian filter of order 1.

A. Extension to Higher Bit Rate

In order to show that the model is future-proof and that its performance is independent of the bit rate, Fig. 3 shows the comparison simulations vs analytical model, in terms of SNR and BER, in the same conditions as in Fig. 2, but for a higher bit rate of 200 Gbps. To be able to show a meaningful BER we have in this case set $N_0 = 0.6 \cdot 10^{-19}\ W^2/Hz$. The estimation error is still excellent both in terms of SNR and BER, for both supergaussian filter orders and for both equalizers.

B. Effect of RIN

As mentioned in the previous Section II, in the estimation of the SNR, our model relies on the approximation that the PSD

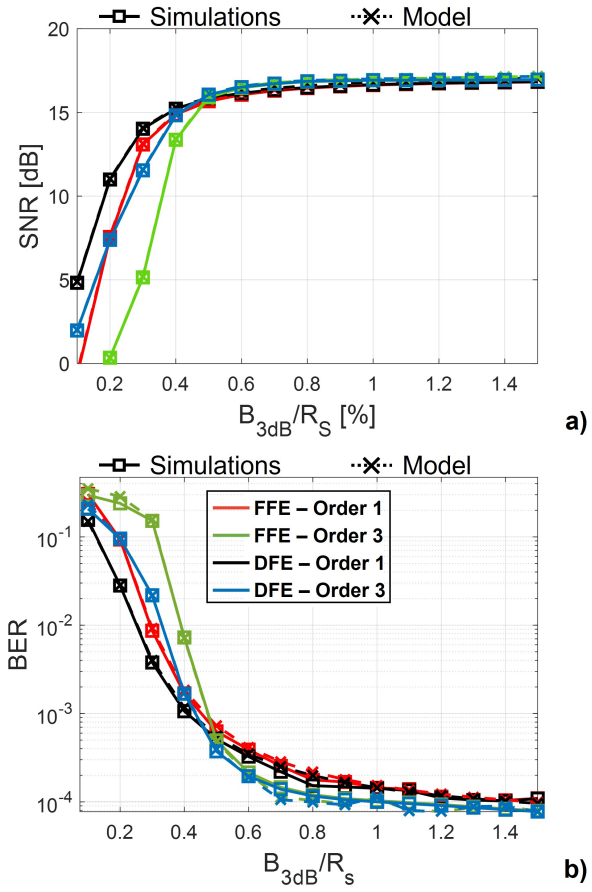

Fig. 3. a) SNR and b) BER obtained through time domain simulations (solid, squares) and through the proposed analytical model (dashed, crosses) as a function of the ratio between the supergaussian filter 3 dB bandwidth B_{3dB} and the symbol rate R_s for a 100 GBaud 4-PAM system, using both FFE (red and green) and DFE (black and blue) equalization. The supergaussian filter order is 1 for black and red curves and 3 for blue and green curves. The legend in b) applies to a) as well.

of the shot noise is proportional to the average useful signal power and the RIN PSD is proportional to the average power squared. However, a more accurate model should assume that they are proportional to the instantaneous power, and this is what we have introduced in the time-domain simulations with which we want to validate our analytical model. This approximation might become inaccurate when the noise levels are sufficiently high to break the validity of the assumption, especially for the RIN, as it is proportional to the square of the instantaneous signal power. Thus, we have performed a sort of "stress test" of the proposed model varying the RIN coefficient in the range from -150 dB/Hz up to -120 dB/Hz with ER = 12 dB and P_{TX} = 0 dBm (OMA = 2.46 dBm). The upper RIN value is clearly not physical (i.e. much higher than typical commercial laser values) but was used in simulation only as a model double check. Moreover, to check the applicability of our model to any data rate, we have increased the symbol rate of the simulated 4-PAM IMDD system to 56 GBaud, a typical value for modern 100G/lane solutions. The results of the comparison with the time domain simulator in terms of $\Delta SNR = SNR_{model} - SNR_{sim}$ in dB are depicted in Fig. 4a.

The contour plot shows an estimation error very close to 0 dB across the whole investigated space of parameters for both FFE (solid) and DFE (dashed) scheme, with values above 0.05 dB only for very strongly bandlimited conditions ($B_{3dB}/R_s = 0.1$) or for filter bandwidth larger than the baud rate ($B_{3dB}/R_s > 1$). In this latter case, a higher estimation error is to be expected: when there is no bandwidth limitation, the impact of receiver equalization is reduced and so is the time averaging effect associated with the equalizer FIR filters. The average power assumption our model is based upon is, thus, broken and the estimation becomes less accurate. Nevertheless, maximum errors of the order of 0.2 dB are still acceptable. Similarly, the evolution of the corresponding BER (obtained as the average of the three per-eye BER) in Fig. 4b shows a remarkable agreement between the two methods with FFE equalization, with negligible mismatch only for BER below 10^{-5}, due to the limited simulated number of transmitted bits, and for B_{3dB}/R_s ratios larger than 1, where the SNR estimation error slightly increases. Similar results were obtained with DFE equalization, not shown here due to space limitations.

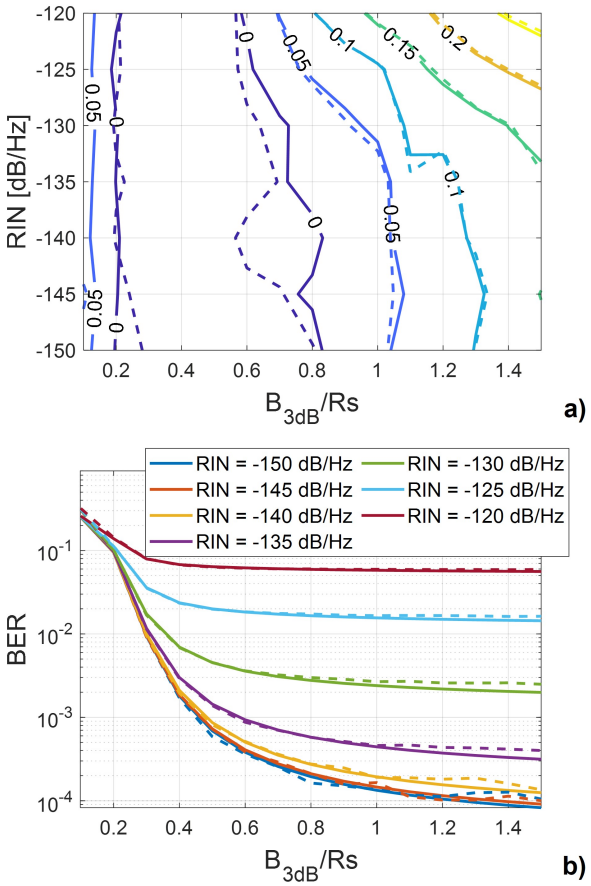

Fig. 4. a) ΔSNR difference in dB between the analytical and simulated results for a 56 GBaud 4-PAM IMDD system, as a function of the RIN coefficient and of the ratio between the filter 3 dB bandwidth and the symbol rate for both FFE (solid) and DFE (dashed) equalization. b) BER evolution obtained through analytical model (solid) and time domain simulations (dashed) as a function of the ratio between the filter 3 dB bandwidth and the symbol rate for several values of the RIN coefficient and FFE equalization.

C. Chromatic Dispersion Approximation

It is well known that, in terms of field propagation, the linear transfer function of a single mode fiber (SMF) in presence of chromatic dispersion only, can be described by the following expression:

$$H_{SMF}(f) = e^{j\pi cDL\cdot\frac{(f-f_c)^2}{f_c^2}} \tag{11}$$

where L is the fiber length, f_c is the central frequency of the optical signal and D is the CD coefficient. Unfortunately, the received IMDD electrical signal after the photodiode is proportional to the modulus square of the field and, thus, the CD effect becomes intrinsically nonlinear and thus the end-to-end electrical transfer function cannot be directly related to Eq. 11. Nevertheless, in [17] a small signal analysis is carried out that allows to approximate Eq. 11 under the assumptions that the modulation amplitude is small compared to average signal power (i.e. that the M-PAM outer extinction ratio is small) and that the transmitter amplitude modulation is chirpless. The approximated small signal electrical-to-electrical transfer function of the system under chromatic dispersion effect only can be expressed as:

$$H_{CD}(f) = cos\left[\pi cDL\left(\frac{f}{f_c}\right)^2\right] \tag{12}$$

Including $H_{CD}(f)$ in our system, the $H_{ch}(f)$ function in Fig. 1 and in Eq. 9 becomes now:

$$H_{ch}(f) = H'_{ch}(f)\cdot H_{CD}(f) \tag{13}$$

where $H'_{ch}(f)$ is the channel frequency response due to the optoelectronic bandwidth limitations without CD (i.e. the super-Gaussian filter used in all our previous analyses). Note that the RIN contribution, as well as the useful signal, is now filtered also by the CD equivalent transfer function.

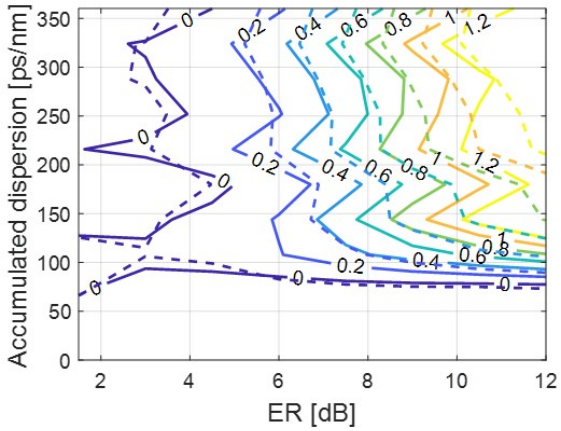

Fig. 5. ΔSNR difference in dB between the analytical and simulated results as a function of the accumulated dispersion and extinction ratio for both FFE (solid) and DFE (dashed) equalization.

Fig. 5 shows the comparison between the analytical model and the time domain simulations in terms of ΔSNR as a function of the accumulated dispersion ($D\cdot L$) and ER, when $RIN = -140$ dB/Hz, $P_{TX} = 0$ dBm, $B_{3dB}/R_s = 0.4$ and $\lambda_c = c/f_c = 1310$ nm. The model estimation accuracy is excellent for accumulated dispersion up to 90 ps/nm and for ER up to 5 dB regardless of the considered equalization scheme. For a given value of the accumulated dispersion above 100 ps/nm the estimation error increases with ER, as the small signal approximation is gradually broken. The small signal approximation used in the derivation of Eq. 12, in fact, is based on the assumption that the amplitude modulation is small compared to the signal intensity, but increasing the ER results in a larger modulation amplitude. Moreover, the SNR discrepancy, that translates to a BER estimation error according to Eq. 10, is also due to the fact that at 50 GBaud, $B_{3dB}/R_s = 0.4$ and for accumulated dispersion in excess of 100 ps/nm the BER is already above $3\cdot 10^{-2}$ in a range where the simulator equalizer does not function properly and the system performance is of little interest. On the other hand, for a given ER an increase of the accumulated dispersion above 150 ps/nm does not alter the estimation accuracy substantially, indicating that the only limitation to our analytical model is the aforementioned small signal approximation. Nevertheless, the accuracy of our model is very good, with SNR estimation error very close to 0 dB, even for ER values well above 6 dB, when considering typical PON lengths up to 20 km (up to 77 ps/nm accumulated dispersion when D=3.85 $ps/(nm\cdot km)$). In this regard, it is worth mentioning that we chose D=3.85 $ps/(nm\cdot km)$ as a worst case dispersion coefficient for O-band (as indicated in ITU.T G9804 50G-PON guidelines).

D. Avalanche Photodetection

In some applications where a higher receiver IMDD sensitivity is needed [18], such as in Passive Optical Networks (as described in the last Section of this paper), APDs are used to generate an electrical gain but also introducing an additional contribution to the total shot noise produced in the photodetection process. In fact, the PSD of the avalanche shot noise is given by:

$$S_{shot}(f) = G^2 F q \overline{P_{RX}} R^{-1} \tag{14}$$

where $\overline{P_{RX}}$ is the average received optical power that we use in our model to approximate the instantaneous received optical power, G is the gain of the photodiode, F is its excess noise factor, q is the electron charge and R is the photodiode responsivity. In the following analysis we have considered APD parameters assuming 50G-class devices [6], [19] with $G = 5$ dB, $F = 3$ dB, $R = 0.7$ A/W and $B_{3dB}/R_s = 0.7$. Fig. 6 shows the SNR obtained with the two methods as a function of the received optical power for a 56 GBaud 4-PAM modulation when the transmitted power is 0 dBm and ER is 3 dB or 6 dB. We show here only the results using FFE equalization, since when the ratio B_{3dB}/R_s is equal to 0.7 no significant SNR difference can be observed when DFE is used.

Fig. 6 highlights again an excellent match between the SNR estimated by the proposed analytical model and that computed through time domain simulations, regardless of the ER value. The estimation error is about 0.02 dB for each simulated P_{RX} value.

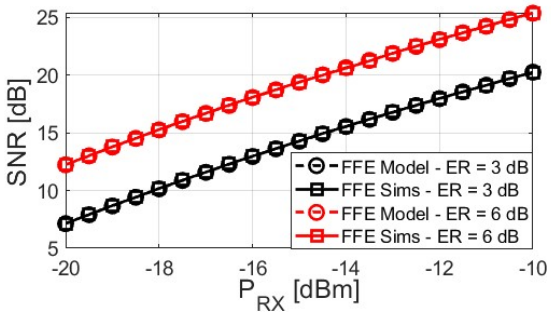

Fig. 6. SNR obtained through time domain simulations (solid, squares) and through the proposed analytical model (dashed, circles) as a function of the received optical power using 56 GBaud 4-PAM with FFE equalization. Transmitted power is 0 dBm and ER is 3 dB (black) or 6 dB (red).

E. Equalizer Memory

As the proposed analytical model is based on a derivation [14] that assumes infinitely long equalizer memory, in the previous Sections we presented results obtained in comparison to time domain simulations performed using a high number of taps (see Table I). Since equalizer convergence is usually sought with the shortest possible memory to reduce complexity and cost of the electronic implementation of the equalization scheme, here we investigate on the prediction accuracy of our model in comparison to more realistic versions of the equalization algorithm, varying the number of taps for both the FFE and DFE stage in the simulator.

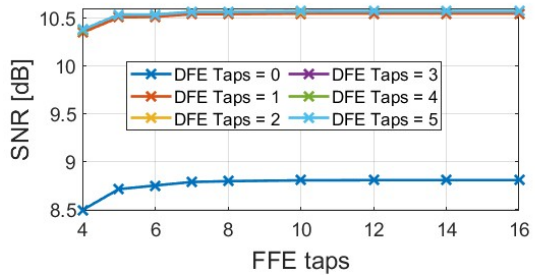

Fig. 7. SNR obtained through time domain simulations as a function of the number of FFE taps for several numbers of DFE taps. P_{TX} = 0 dBm and B_{3dB}/R_s = 0.25.

Fig. 7 shows the SNR at the output of the equalizer as a function of the number of taps for a simulated 56 GBaud 4-PAM transmission with P_{TX} = 0 dBm and a strong bandwidth limitation with $B_{3dB}/R_s = 0.25$. When pure FFE equalization is used a number of taps as low as 10 is sufficient for perfect equalizer convergence and, even using 4 taps the SNR estimation error is only about 0.3 dB. Moreover, when DFE is used 10 taps for the FFE stage of the DFE equalizer are required to achieve optimum performance, whereas only 2 taps are enough for the DFE stage. Since these numbers of taps are those typically used in practical implementations of receiver adaptive equalizers, we can conclude that a reasonable number of taps in the simulator (and therefore in the experiments) is enough to achieve the same performance predicted by the analytical tool, and thus the validity of our analytical model is good also in the finite-length FIR practical cases.

IV. Application Examples

In this Section, we apply our analytical model to the analysis of the specific use cases on next generation ultra-high speed Passive Optical Network (PON) and on systems based on MMF and VCSEL for DCI applications.

A. PON Simulations

Standardization efforts for next generation PONs are being focused to the next big step in transmission speed [6]. Although it is yet not clear whether the next target bit rate will be 100G or 200G, and if the traditional IMDD-based PON architecture will transition to more complex yet advantageous coherent solutions [2], in the mid term there will for sure be the need to upgrade current PON capacity to, at least, 100 Gbps/λ. In the PON environment this is usually intended as a gross target bit rate, thus including the overhead associated to the employed forward error correction (FEC) algorithm. The hard-decision FEC (HD-FEC) defined in the 50G PON standard sets the pre-FEC BER threshold to 10^{-2}, but even soft-decision FECs (SD-FECs) might be selected in future PON standards raising the BER threshold to $1.9 \cdot 10^{-2}$ [20]. Moreover, current standards require at least 29 dB optical power budget (OPB) for N1 class PON. This physical layer requirement is hardly going to be modified and will be the main challenge in future versions of PON due to the reduced sensitivity of IMDD systems at such high bit rates. Fig. 8 shows a simplified setup

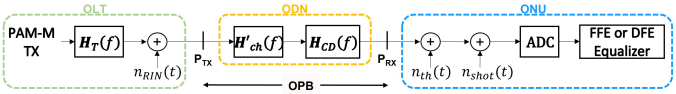

Fig. 8. Simplified scheme of the PON under investigation.

of a downstream PON with APD-based detection, relating the optical line terminal (OLT), the optical distribution network (ODN) and the optical network unit (ONU) to the building blocks of our analytical model. As in the previous Section, we have considered APD parameters assuming 50G-class devices [6], [19] with G = 5 dB, F = 3 dB and R = 0.7 A/W. The OPB is defined across the ODN as the ratio between the transmitted optical power P_{TX} and the received optical power P_{RX} at a given target BER level. In our analysis, we set the transmitted power to 11 dBm, a typical value often used in PONs to avoid the inset of single-wavelength nonlinear Kerr effects. Moreover, we assume the PON is operated in the O-band where the chromatic dispersion effect is small. Thus, in our approximation of the CD transfer function we fixed the dispersion parameter D to 3.85 $ps/(nm \cdot km)$, corresponding to the upper O-band wavelength of the grid plan of recently standardized 50G-PON [6]. Fig. 9 shows the comparison between model and simulations in terms of SNR and corresponding BER as a function of the received optical power for a 50 GBaud PON with three values of the ER, in back-to-back and with 25 km of single mode fiber. The ratio B_{3dB}/R_s = 0.7, thus we only show results for FFE equalization as no significant SNR difference can be observed when DFE is used. Fig. 9a highlights again a perfect

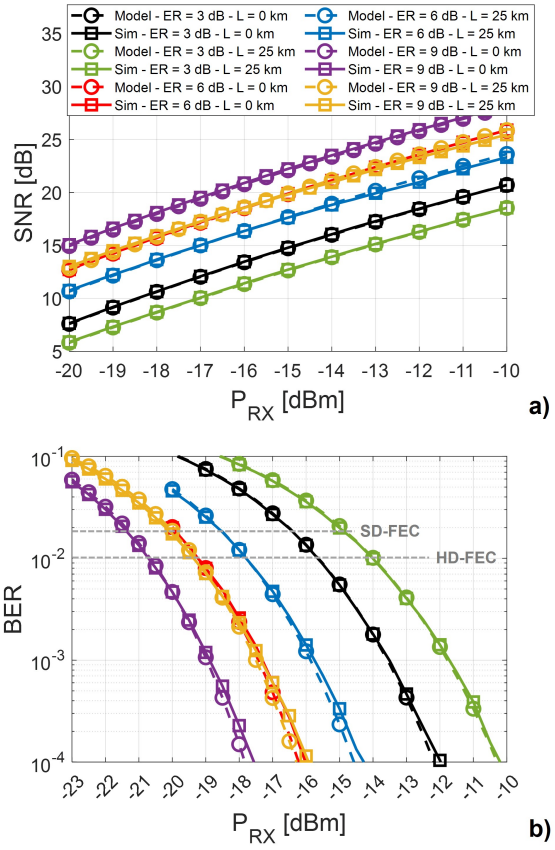

Fig. 9. a) SNR and b) corresponding BER obtained through time domain simulations (solid, squares) and through the proposed analytical model (dashed, circles) as a function of the received optical power using 50 GBaud 4-PAM (i.e. 100 Gbps) with FFE equalization in back-to-back (black, green) and with 25 km SMF in O-band (red, blue). Transmitted power is 11 dBm, ER is 3 dB (black, red), 6 dB (green, blue) or 9 dB (purple, orange). Legend in a) applies to b) as well.

agreement of the model with the simulations. A very small estimation error of about 0.3 dB on the SNR can be observed for received optical power above -14 dBm in the configuration with 25 km SMF and ER greater than 6 dB, where the small signal approximation in Eq. 12 starts to become inaccurate. In Fig. 9b an excellent match on the sensitivity curves can also be observed. A slight mismatch of about 0.25 dB on the received optical power occurs at BER=10^{-4} only for the configurations with ER above 6 dB. However, at the BER levels of interest around 10^{-2} the model is very accurate and shows two requirements for a PON with 25 km SMF and 100 Gbps 4-PAM modulation. To achieve the required 29 dB OPB the ER (typically the ER associated to a directly modulated laser or an electroabsorption modulated laser in the PON scenario) should be at least 6 dB and the use of a SD-FEC is necessary.

B. PON Experiments

As a further validation of the model we also present here the comparison between our analytical tool and a set of previously performed experiments in the PON scenario presented in [21]. The effect of the quantization noise associated to the ADC is taken into account in the model, as in the experiments we use a 100 Gsample/s real-time oscilloscope (RTO) with 33 GHz bandwidth. Eq. 13 becomes $H_{ch}(f) = H'_{ch}(f) \cdot H_{CD}(f) \cdot H_{ADC}(f)$, where $H_{ADC}(f)$ is the transfer function of the ADC modeled as a supergaussian filter of order 3 with 33 GHz 3dB cutoff frequency.

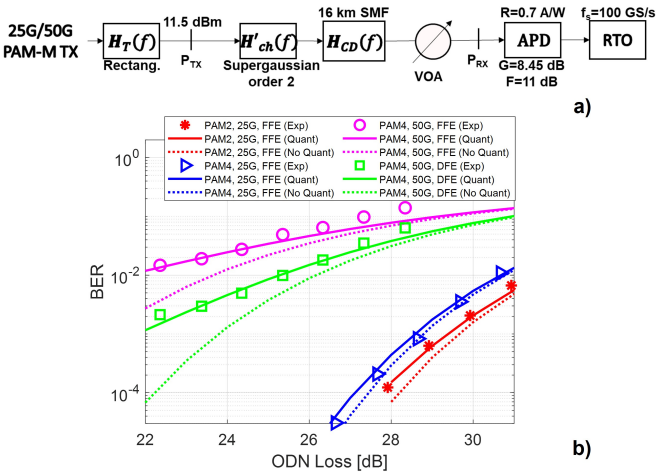

Fig. 10. a) Block diagram abstraction of the experimental setup with main system parameters. b) BER as a function of the received optical power for 25G 2-PAM with FFE (red,asterisk), 25G 4-PAM with FFE (blue, triangle) and 50G 4-PAM with FFE (magenta, circle) and DFE (green, square), obtained through experiments (markers) analytical model with quantization (solid) and analytical model without quantization (dot).

Fig. 10a shows the block diagram of the experimental setup with the main system parameters. We assume here a linear modulation that generates equally spaced 4-PAM levels in terms of instantaneous power. Fig. 10b shows the BER as a function of the received optical power for 2-PAM and 4-PAM transmission at 25G and 50G over 16 km SMF. In the DSP for experimental data the number of taps was set to 20 and 5, respectively for FFE and DFE. The other main system parameters are $R = 0.7$ A/W, $N_0 = 2 \cdot 10^{-21}$ W^2/Hz, $P_{TX} = 11.5$ dBm, $ER = 5$ dB, $RIN = -140$ dB/Hz, $G = 8.45$ dB, $F = 11$ dB, $D \cdot L = -3.2ps/nm$, $ENOB = 5$ and $f_s = 100$ GS/s. Moreover, the bandlimited experimental system is emulated in the model as a supergaussian filter $H'_{ch}(f)$ of order 2 with 8.5 GHz 3 dB bandwidth, obtained through fitting on the experimental frequency response shown in [21], and the BER curves shown in Fig. 10b. At 25G the match between model and experiments is nearly perfect and only a marginal impact of the quantization noise can be observed. At 50G, on the other hand, a BER floor in the experimental results produces a large estimation error for decreasing ODN loss. However, the mismatch reduces remarkably when we include the effect of the quantization noise in the model, showing the importance of taking also this effect into account.

Fig. 11. Block diagram of the simulated VCSEL-MMF link.

C. VCSEL+MMF DCI Systems

Thanks to its advantages in terms of cost and simplicity MMF is still largely employed in short-reach DCI, over distances up to a few hundred meters, coupled with VCSELs. Here we apply our analytical model to the setup in Fig. 11, where $H_T(f)$ represent the rectangular shaping filter at the transmitter, $H_{VCSEL}(f)$ is the measured transfer function of the VCSEL with 25 GHz 3-dB cut-off frequency, $H_{MMF}(f)$ is the transfer function calculated as in [5], [23] at 850 nm. Lastly, $H_{RX}(f)$ is the frequency response of the photodiode described as an 8th order Butterworth filter with 26 GHz 3-dB cutoff frequency. Fig. 11 shows where the $n_{RIN}(t)$, $n_{shot}(t)$ and $n_{th}(t)$ contributions, respectively from RIN, shot and thermal noise are added in the simulations. The main parameters are $R_S = 25$ GBaud, $R = 0.5$ A/W, $N_0 = 1.6 \cdot 10^{-21}$ W^2/Hz, $P_{TX} = -1.75$ dBm, $ER = 3$ dB and $RIN = -140.5$ dB/Hz.

Fig. 12a shows the SNR predicted by the time-domain simulator compared to the SNR generated analytically for 200 OM3 MMFs and a 50G 4-PAM transmission over 150 m MMF link. Both for FFE and DFE equalization the estimation error is below 0.1 dB for all the 200 cases (see Fig. 12b).

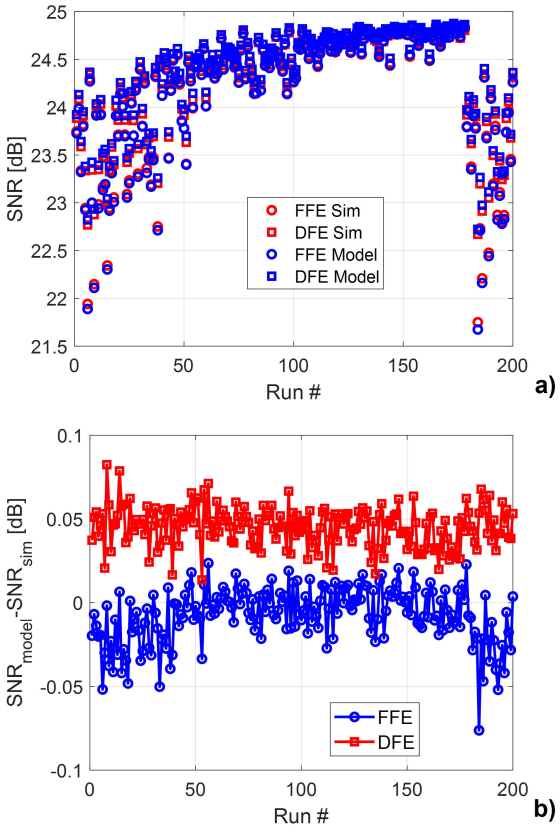

Fig. 12. a) SNR of the VCSEL+MMF DCI system obtained through simulations (red) and analytically (blue) for FFE (circle) and DFE (square). b) SNR estimation error between simulations and analytical model for FFE (blue, circle) and DFE (red, square).

V. Discussion and Conclusions

We have presented an analytical model for fast performance estimation of IMDD-based communications systems affected by RIN, shot and APD noise, thermal noise, quantization noise, chromatic dispersion and bandwidth limitations. The tool requires knowledge of the linear transfer function of the channel and can provide accurate SNR and BER prediction with over 400 times reduction in computation time compared to full time domain simulations.

We have evaluated the realm of applicability of our model focusing on 4-PAM modulation with FFE and DFE equalization for 50G and 100G target bit rates, showing SNR estimation errors below 0.1 dB for a wide range of RIN, shot noise and ER levels, regardless of the bandwidth limitation imposed by the channel. We also equipped our model with the possibility to take into account the effect of CD showing very good agreement with simulations for accumulated dispersion up to 360 $ps/(nm \cdot km)$ and ER up to 9 dB.

Lastly, we have applied and validated our analytical approach in two specific scenarios: a PON based on 4-PAM and APD photodetection and a MMF-based DCI link. The comparison with simulations reveals the need for at least 6 dB ER and advanced SD-FEC algorithms for the system to be able to meet the 29 dB OPB requirement imposed by current N1 PON class standard at 100 Gbps/λ . Furthermore, the introduction of the quantization effect in the model allowed to obtain an excellent match with experimental measurements on 25G and 50G transmission. A very good agreement with 25 GBaud 4-PAM simulations in a DCI environment was also obtained, with estimation errors of the order of 0.05 dB.

We believe that the proposed model is applicable to a wide range of current and future IMDD ultra high speed transmission and that it can be very useful, for instance, when a standardization body has to define a new transmission standard, and thus have to theoretically assess the expected performance in presence of different types of bandwidth limitations and noise effects. The model can be further extended to consider (but we cannot show the results here due to space limitations):

1) unequally spaced M-PAM levels, for instance to study inaccuracies in M-PAM generation
2) lasers with chirp as the small signal approximation we used in Eq. 12 assumes a chirpless modulation and a linear fiber. There are models (again under the "small modulation" assumption) that enable the computation of an analytical transfer function also for transmitter chirp and nonlinear self-phase modulation along the fiber.

Regarding the limitations of our model, the impairments that it cannot directly handle are the error propagation effect that can occur in DFE-based equalization, the penalty due to finite number of taps of the equalizers and the nonlinear distortion in the transmitted eye diagram associated, for instance, to the time-skew that can be present in directly modulated lasers [24], [25] or in other nonlinear devices [26]. Concerning DFE error propagation, strategies such as pre-coding [27] and bit-interleaving [28] have been proposed to reduce the penalty caused by this effect, especially when DFE is combined with

FEC, as in most modern IMDD systems. In respect to the finite-tap equalizer penalty, in [29] the Authors have recently proposed a similar analytical tool in the scenario of optically amplified transmission over several tens of km, which can account for an arbitrary number of taps of the equalizer, and also for the residual inter-symbol interference that cannot be compensated through DSP. However, it does not take into account RIN whereas, similarly to ours, it is based on the linear approximation of the chromatic dispersion effect. Besides, we showed that after few equalizer taps, the penalty with respect to infinite-long equalizer becomes negligible. Moreover, in our paper we focus on the effect of several parameters, such as the modulation extinction ratio, that are not analyzed in [29].

An open-access free version of the Matlab code implementing the presented analytical model can be found in [15], [16].

ACKNOWLEDGMENT

This work was carried out under a research contract with Cisco Photonics and in the PhotoNext initiative at Politecnico di Torino. www.photonext.polito.it. Pablo Torres-Ferrera acknowledges the support of *Secretaría de Educación, Ciencia, Tecnología e Innovación* (SECTEI), Mexico City, and the University of Cambridge, United Kingdom. For the purpose of open access, the author has applied a Creative Commons Attribution (CC BY) license to any Author Accepted Manuscript version arising. Data underlying the results presented here are available at https://doi.org/10.17863/CAM.97164.

REFERENCES

[1] E. Maniloff, S. Gareau and M. Moyer, "400G and Beyond: Coherent Evolution to High-Capacity Inter Data Center Links," in *Optical Fiber Communications Conference and Exhibition (OFC)*, San Diego, CA, USA, 2019, pp. 1-3.

[2] G. Rizzelli, A. Nespola, S. Straullu, F. Forghieri and R. Gaudino, "Scaling Laws for Unamplified Coherent Transmission in Next-Generation Short-Reach and Access Networks," *J. Lightwave Technol.*, vol. 39, no. 18, pp.5805-5814, 2021.

[3] G. Rizzelli, F. Forghieri and R. Gaudino, "Experimental Demonstration of Real-Time 400G Coherent Transmission Over 300m OM3 MMF," in *Proc. OFC*, San Diego, CA, USA, 2022.

[4] M. S. Faruk, X. Li, D. Nesset, I. N. Cano, A. Rafel and S. J. Savory, "Coherent Passive Optical Networks: Why, When, and How," *IEEE Communications Magazine*, vol. 59, no. 12, pp. 112-117, 2021

[5] G. Rizzelli, P. Torres-Ferrera, F. Forghieri, A. Nespola, A. Carena and R. Gaudino, "Coherent Communication Over Multi Mode Fibers for Intra-Datacenter Ultra-High Speed Links," in *Journal of Lightwave Technology*, vol. 40, no. 15, pp. 5118-5127, 1 Aug.1, 2022.

[6] P. Torres-Ferrera, F. Effenberger, M. S. Faruk, S. J. Savory and R. Gaudino, "Overview of high-speed TDM-PON beyond 50 Gbps per wavelength using digital signal processing," in *Journal of Optical Communications and Networking*, vol. 14, no. 12, pp. 982-996, 2022.

[7] M. S. -B. Hossain et al., "Probabilistic Shaping for High-Speed Unamplified IM/DD Systems With an O-Band EML," in *J. Lightwave Technol.*, doi: 10.1109/JLT.2023.3263039, 2023.

[8] X. Pang et al., "200 Gb/s Optical-Amplifier-Free IM/DD Transmissions using a Directly Modulated O-band DFB+R Laser targeting LR Applications," in *J. Lightwave Technol.* doi: 10.1109/JLT.2023.3261421, 2023.

[9] P. Torres-Ferrera, G. Rizzelli, H. Wang, V. Ferrero and R. Gaudino, "Experimental Demonstration of 100 Gbps/λ C-Band Direct-Detection Downstream PON Using Non-Linear and CD Compensation with 29 dB+ OPL Over 0 Km–100 Km," in *J. Lightwave Technol.*, vol. 40, no. 2, pp. 547-556, 2022.

[10] H. Taniguchi et al., "High-capacity IM-DD transmission in O-band using advanced maximum likelihood sequence estimation methods," in *J. Lightwave Technol.*, doi: 10.1109/JLT.2023.3253792, 2023.

[11] P. Torres-Ferrera et al., "Statistical Analysis of 100 Gbps per Wavelength SWDM VCSEL-MMF Data Center Links on a Large Set of OM3 and OM4 Fibers," in *J. Lightwave Technol.*, vol. 40, no. 4, pp. 1018-1026, Feb. 15, 2022.

[12] V. Curri, M. Cantono and R. Gaudino, "Elastic All-Optical Networks: A New Paradigm Enabled by the Physical Layer. How to Optimize Network Performances?," *J. Lightwave Technol.*, vol. 35, no. 6, pp. 1211-1221, 15 March, 2017.

[13] G. Rizzelli, P. Torres-Ferrera and R. Gaudino, "An Analytical Model for Coherent Transmission Performance Estimation after Generic Jones Matrices," in *J. Lightwave Technol.*, vol. 41, no. 14, pp. 4582-4589, July 2023.

[14] Robert F.H. Fischer, "Linear Equalization," in *Precoding and Signal Shaping for Digital Transmission*, New York, NY, USA: Wiley-Interscience, 2002, ch. 2, sec. 2.2.4, pp. 35-43.

[15] G. Rizzelli, P. Torres-Ferrera, F. Forghieri and R. Gaudino, "Analytical Model for IMDD Transmission Systems". Zenodo, Aug. 31, 2023. [Online]. Available: https://doi.org/10.5281/zenodo.10018546.

[16] G. Rizzelli, P. Torres-Ferrera, F. Forghieri and R. Gaudino, "Analytical Model for IMDD Transmission Systems". Codeocean, Aug. 31, 2023. [Online]. Available: https://codeocean.com/capsule/3338093/tree/v1.

[17] J. Wang and K. Petermann, "Small signal analysis for dispersive optical fiber communication systems," in *Journal of Lightwave Technology*, vol. 10, no. 1, pp. 96-100, Jan. 1992.

[18] M. Nada, T. Yoshimatsu, Y. Muramoto, T. Ohno, F. Nakajima and H. Matsuzaki, "106-Gbit/s PAM4 40-km Transmission Using an Avalanche Photodiode With 42-GHz Bandwidth," in *Proc. OFC*, San Diego, CA, USA, 2018.

[19] E. Harstead et al., "From 25 Gb/s to 50 Gb/s TDM PON: transceiver architectures, their performance, standardization aspects, and cost modeling," in *Journal of Optical Communications and Networking*, vol. 12, no. 9, pp. D17-D26, Sep. 2020.

[20] R. Borkowski et al., "FLCS-PON – A 100 Gbit/s Flexible Passive Optical Network: Concepts and Field Trial," in *Journal of Lightwave Technology*, vol. 39, no. 16, pp. 5314-5324, Aug. 2021.

[21] P. Torres-Ferrera, H. Wang, V. Ferrero, M. Valvo and R. Gaudino, "Optimization of Band-Limited DSP-Aided 25 and 50 Gb/s PON Using 10G-Class DML and APD," in *Journal of Lightwave Technology*, vol. 38, no. 3, pp. 608-618, Feb. 2020.

[22] A. Napoli et al., "Digital Compensation of Bandwidth Limitations for High-Speed DACs and ADCs," in *Journal of Lightwave Technology*, vol. 34, no. 13, pp. 3053-3064, July 2016.

[23] J. M. Castro, R. Pimpinella, B. Kose and B. Lane, "Investigation of the Interaction of Modal and Chromatic Dispersion in VCSEL-MMF Channels," in *Journal of Lightwave Technology*, vol. 30, no. 15, pp. 2532-2541, Aug. 2012.

[24] A. G. Reza, et al., "Single-Lane 54-Gbit/s PAM-4/8 Signal Transmissions Using 10G-Class Directly Modulated Lasers Enabled by Low-Complexity Nonlinear Digital Equalization," in *IEEE Photonics Journal*, vol. 14, no. 3, pp. 1-9, 2022.

[25] L. Minelli, F. Forghieri, A. Nespola, S. Straullu and R. Gaudino, "A Multi-Rate Approach for Nonlinear Pre-Distortion Using End-to-End Deep Learning in IM-DD Systems," in *Journal of Lightwave Technology*, vol. 41, no. 2, pp. 420-431, 2023

[26] J. Molina-Luna, R. Gutiérrez-Castrejón, D.E. Ceballos-Herrera, "Alternative to Super-PON downstream transmitter using a directly-modulated SOA," *Opt Quant Electron*, 54, 830, 2022.

[27] Y. Lu, L. Li, L. MA and Y. Zhuang,"Elimination of DFE Error Propagation and Post-FEC Error Floor (Precoding 2.0)," IEEE 802.3 100 Gb/s, 200 Gb/s, and 400 Gb/s Electrical Interfaces Task Force, Vancouver, BC, Canada, Mar. 7, 2019. [Online] Available: https://www.ieee802.org/3/ck/public/19_03/lu_3ck_01_0319.pdf.

[28] A. Mahadevan et al., "Impact of DFE on Soft-Input LDPC Decoding for 50G PON," 2021 Optical Fiber Communications Conference and Exhibition (OFC), San Francisco, CA, USA, 2021.

[29] P. Zhu, Y. Yoshida, A. Kanno and K. -i. Kitayama, "Analysis and Demonstration of Low-Complexity Joint Optical-Electrical Feedforward Equalization (OE-FFE) For Dispersion-Limited High-Speed IM/DD Transmission," in *Journal of Lightwave Technology*, vol. 41, no. 2, pp. 477-488, Jan. 2023.